Desalination and Water Treatment
www.deswater.com

doi: 10.5004/dwt.2021.27062

222 (2021) 219–236
May

Retention and release of the orange azo dyes by the chitosan-clay beads in aqueous solutions

Sarra Kabbadj, Mohamed Hajjaji*, Abdelhakim Alagui

Laboratoire de Physico-chimie des Matériaux et Environnement, Faculté des Sciences Semlalia, Université Cadi Ayyad, B.P. 2390, Av. Pce My Abdellah, 40001 Marrakech, Morocco, Fax: +212 5 24 43 74 08; emails: hajjaji@uca.ma (M. Hajjaji), sarra.kabbaj@gmail.com (S. Kabbadj), alagui@uca.ac.ma (A. Alagui)

Received 4 July 2020; Accepted 24 January 2021

ABSTRACT

Retention and release of the azo dyes (orange II and orange G) by the beads of shell shrimp-derived chitosan (50% wt/wt) and stevensite-rich clay or illite–kaolinitic clay were investigated by using the Fourier-transform infrared spectroscopy and the scanning electron microscopy, and by adopting the response surface methodology. The adsorption kinetics and the isotherms were measured. The results showed that the dyes retention occurred spontaneously ($-40 < \Delta G° < -35$ kJ/mol at 298 K), and the ($NHCOCH_3$), (CH_2OH), and (NH_3^+) moieties of the chitosan were the main sites of the beads involved in the retention process. The adsorption kinetics was relatively fast, and the maximum uptakes at 298 K were in the 90–135 mg/g range. The weights of the effects of the operating factors on the desorption efficiency of both dyes followed the order: pH > temperature > ionic strength. The beads were reusable, but because of their gradual peeling off, the adsorption ability declined from 25% to 60% at the third adsorption–desorption cycle.

Keywords: Chitosan-clay beads; Azo dyes; Retention/Release; Characterization; Response surface methodology

1. Introduction

Azo dyes such as the orange II and the orange G are water-soluble compounds consisting of the chromophore group (–N=N–), aromatic rings, and the SO_3H moiety [1]. They make up approximately 70 wt.% of the total dyestuffs [2], and they are commonly used in dyeing textile and leather, among others. Up to about 10 wt.% of these dyes are found in the dyeing plants effluents [3]. The azo dyes resist biological decomposition and photodegradation [4]. So, their presence in wastewaters threatens the purity of the surface water and the groundwater and has detrimental effects on the health of human beings and living species [5]. Thus, particular attention has been paid to their immobilization.

Adsorption is considered as an adequate technique for the removal of dyes from aqueous solutions because of its efficiency and implementation facility [2]. The commercial adsorbent that is traditionally used is activated carbon, but its manufacturing and regeneration are costly processes [6].

To find inexpensive and efficient adsorbents for the dyes removal from aqueous solutions, numerous adsorption studies have been conducted on natural and modified clays [7], and on polymers-based composites [8]. Clay minerals of the smectite group, such as montmorillonite and stevensite, are efficient natural adsorbents. The adsorption efficiency of these minerals is attributed to their high surface area and cation exchange capacity, and to the possible expansion of their interlayer spaces [9]. However, because of

* Corresponding author.

their anionic character, these materials are not suitable for the retention of the azo dyes, which are anionic compounds.

Chitosan, which is a chitin derivative polymer, is a non-toxic and biodegradable polysaccharide. In acid solutions the amino-groups of the chitosan are the object of protonation, thus forming positive active sites. Therefore, it can be used as an adsorbent for anionic chemical contaminants, such as azo dyes and oxyanions. Also, it is suitable for the synthesis of new adsorbents [10].

As acid–soluble polymer, the chitosan in acid aqueous solutions cannot be easily isolated. This drawback can be overcome by its association with swelling clay minerals. Thus, composites of montmorillonite and chitosan have been the subject of many studies dealing with their adsorption ability [11–21]. However, too little attention has been paid to the use of the chitosan-montmorillonite beads for the uptake of anionic dyes [22]. In addition, the use of expandable clay minerals other than montmorillonite has been ignored. Thus, in this study, the beads composed of shell shrimp-derived chitosan and stevensite-rich clay (swelling clay) or illite–kaolinitic clay (non-swelling clay) were prepared and their abilities to retain and release the orange II and the orange G azo dyes were investigated.

2. Materials and methods

2.1. Clays

The clay materials used were collected from the clay pits located at the Tetouan-Hoceima and Fès-Boulmane provinces (Morocco). They were denoted BN2 and RH, respectively. BN2 is composed of an assemblage of clay minerals (kaolinite, illite, and smectite), and RH of stevensite [23]. Carbonates and quartz were the main non-clay minerals found in both clays. The carbonates were eliminated by using a buffer solution of acetic acid and sodium acetate (pH = 4.74). In order to delaminate the swelling clay minerals and to increase their dispersion in aqueous solutions, the carbonate-free clays (particles size < 80 μm) were sodium saturated [24]. The Na-saturated clays, labeled Na-RH and Na-BN2, were stored in a drying oven at 105°C.

2.2. Chitosan

The chitosan was prepared by deacetylation of the chitin, which was extracted from the exoskeleton of local shrimp's shells, following the experimental steps described by Ba et al. [25]. The deacetylation degree (DD) and the molecular weight (MW) of the chitosan (alpha-chitosan) prepared were determined to be 90% and 53,819 g/mol. Details regarding the methods adopted for the DD and MW measurements are given elsewhere [26–28].

2.3. Orange azo dyes

The orange II ($C_6H_{11}N_2NaO_4S$, 350.32 g/mol) and the orange G ($C_{16}H_{10}N_2Na_2O_7S_2$, 452.37 g/mol), labeled here OII and OG respectively, were Merck products (Taufkirchen, Germany) (dye content: 80%). They were provided as a powder, and they were water-soluble (160 and 1 g/L, respectively). The wavelengths of the maximum absorption were 485 and 476 nm for OII and OG, respectively. The values of the pH of the point of zero charge (PZC) of these dyes, which were determined by adopting the salt addition method [29], are given in Table 1.

2.4. Chitosan-clay beads preparation

Based on preliminary tests (not reported here), the beads did not form as the clay portion exceeded that of the chitosan, and the adsorption capacities of the beads composed of 50 wt.% Na-clay were comparable to those of the chitosan beads. Considering these observations, a portion of the chitosan (2 g) was introduced in 60 mL of acetic acid solution (pH = 5) and stirred for 3 h. The limpid solution obtained was mixed with a clay dispersion composed of 2 g of Na-RH or Na-BN2, and 60 mL of acetic acid solution (pH = 5). The mixture was stirred for 1 h at room temperature, and then transferred into the burette. Droplets were drained out of the burette at regular time to fall into a stirred solution of NaOH (0.5 M). The droplets were instantaneously transformed into beads, which were kept in the alkaline solution for 2 h. The beads removed from the alkaline solution were abundantly washed with distilled water and freeze-dried. The textural characteristics and the values of the pH of the PZC of the beads, which were denoted Chit-RH (RH-based beads) and Chit-BN2 (BN2-based beads), are given in Table 1.

2.5. Adsorption kinetics tests

The operating conditions adopted in these tests were chosen on the basis of the following facts: both dyes were quantitatively adsorbed by using small doses of beads and low pH solutions (not below 4.5 in order to prevent the collapse of the structure of the clay minerals). So, beads weighting 0.04 g were introduced in an aqueous solution (200 mL) containing 25 mg/L of the OII dye or the OG dye. The dispersion was continuously and gently stirred at

Table 1
Textural characteristics of the beads studied, and the values of the pH of the point of zero charge (pH_{PZC}) of the beads and the OII and OG dyes

[a]Specific surface area (m^2/g)		[b]Total pore volume (cm^3/g)		[c]Porosity (%)		[d]pH_{PZC}			
Chit-RH	Chit-BN2	Chit-RH	Chit-BN2	Chit-RH	Chit-BN2	Chit-RH	Chit-BN2	OII	OG
45	7	3.6	3.3	88	75	4.8	5	5.1	5.6

[a]Measured by adsorption of N_2 with a Micrometrics FlowSorb III apparatus; [b]$(1/r_a - 1/r_b)$, r_a and r_b are the apparent and the true densities measured by the liquid displacement method; [c]$(1 - r_a/r_b)$; [d]determined by the salt addition method [29].

240 rpm. The temperature and the pH were maintained at 298 K and 4.5, respectively.

Samples were taken out at regular times from the solution prepared, and their absorbance was measured in order to determine the amount of the dye retained. The measurement of the absorbance was performed with the UV-visible spectrophotometer JP-Selecta and using the wavelengths given above. The instantaneous amount of the dye retained was calculated from the equation:

$$q_t = \frac{\left(C_0 - C_t\right)\cdot V}{m} \quad (1)$$

The kinetics data were fitted with the non-linear forms of the pseudo-first and the pseudo-second kinetics order models (Table 2) by using the Addinsoft XLSTAT software. The fitting accuracy was evaluated on the basis of the values of the statistical parameters: correlation coefficient (R^2) and root mean square errors (RMSE) (Table 2). The rate-limiting step was assessed by using the Boyd's model [30] given in Table 2.

2.6. Equilibrium adsorption isotherms

For the plot of the adsorption isotherms, the dye concentrations were varied from 5 to 25 mg/L, and the dose of the beads was fixed at 0.2 g/L. The operating factors adopted were as follows: experiment time: 120 min, stirring: 240 rpm, pH: 4.5, T: 288, 298, and 318 K. The amount of the dye retained was measured as mentioned.

The isotherms curves were fitted with the non-linear forms of the models of Langmuir, Freundlich, and Dubinin–Radushkevich (D–R) (Table 2), and the accuracy of the fitting was evaluated by comparing the values of R^2 and RMSE (Table 2).

The thermodynamic data, namely the Gibbs free energy change, the heat, and the entropy changes, associated with the adsorption processes of the dyes were calculated by using the equations given in Table 2.

2.7. Release of dyes and response surface methodology

The release of the OII and the OG dyes in aqueous solutions by the dye-loaded Chit-RH and Chit-BN2 beads was investigated at a different temperature, pH, and ionic strength by using the response surface methodology, and by adopting the following model [32]:

$$D = a_0 + a_1X_1 + a_2X_2 + a_3X_3 + a_{11}X_1^2 + a_{22}X_2^2 + a_{33}X_3^2 + a_{12}X_1X_2 + a_{13}X_1X_3 + a_{23}X_2X_3 \quad (2)$$

where D is the desorption efficiency calculated from the relation:

$$D = 100\frac{q_d}{q_{\max}} \quad (3)$$

where $q_d = C_rV/m$.

where a_0, a_i, a_{ii}, and a_{ij} are constant. a_i is the weight of the effect of the experimental factor "i" on the desorption efficiency. a_{ij} expresses the weight of the effect of the interaction between "i" and "j" factors on the response "D". a_{ii} is considered as a curve shape parameter. X_i is the coded variable, which is related to the real value (v_i) of the experimental factor "i" according to the equation:

$$X_i = \frac{v_i - v_i^0}{\Delta v_i} \quad (4)$$

where v_i^0 is the "i" factor central value of the investigated domain, and Δv_i is the step variation of the real value of "i"

Table 2
Mathematical expressions of the kinetics and the isotherms models, the statistical parameters and the thermodynamic functions used

Kinetics	
Pseudo-first-order equation	$q_t = q_e\left(1 - e^{-k_1t}\right)$
Pseudo-second-order equation	$q_t = \frac{k_2q_e^2\mathrm{t}}{1 + k_2q_et}$
Boyd's model	$B_t = \left[\sqrt{\pi} - \left(\pi - \frac{\pi^2F(t)}{3}\right)^{1/2}\right]^2$ $F(t) = q_t/q_e$ $F(t) \le 0.85$
Isotherms models	
Langmuir	$q_e = \frac{K_LC_eq_{\max}}{\left(1 + K_LC_e\right)}$
Freundlich	$q_e = K_F\left(C_e\right)^{1/n}$
Dubinin–Radushkevich (D–R)	$q_e = q_{\max}\exp\left(-B\varepsilon^2\right)$ $\varepsilon = RT\left(1 + \frac{1}{C_e}\right)$ $E = \frac{1}{\sqrt{2B}}$
Statistical coefficients	
$R^2 = 1 - \frac{\sum\left(q_m - q_c\right)^2}{\sum\left(q_m - \bar{q}_m\right)^2}$	$\mathrm{RMSE} = \sqrt{\frac{\sum\left(q_m - q_c\right)^2}{n}}$
Thermodynamic functions	
$\Delta G° = -RT\ln K_C$	
$\ln K_C = -\frac{\Delta H°}{RT} + \frac{\Delta S°}{R}$	
$K_C = 10^3 \times 55.5 \times K_L \times M_w$ [31]	

(Δv_I = 0.05 M, Δv_{pH} = 7, and Δv_T = 30°C). X_1, X_2, and X_3 are the coded variables related to I, pH, and T (real variables), respectively. I, pH, and T were varied in the ranges of 0–0.1 M, 5–9, and 20°C–40°C, respectively.

The values of a_0, a_i, a_{ii}, and a_{ij} were determined by using the method of least-square regression. For this purpose, fifteen measurements of the desorption efficiency, which were planned according to the Doehlert design [33], were performed (Table 3).

2.8. Experimental analysis

The Fourier-transform infrared (FT-IR) analysis of the beads was carried out with a Perkin Elmer 1725 spectrometer (Villebon-sur-Yvette, France) functioning in the range of 4,000–400 cm^{-1}. The analysis was done on shaped discs composed of 1 mg of beads and 99 mg of KBr. The deconvolution of the IR bands was performed with the PeakFit v4.12 software (Peak type: Gaussian shape). The accuracy of the deconvolution was assessed based on the correlation coefficient (R^2), the standard error (SE), and the F-statistic.

The microscopic examinations of the beads, which were carbon-coated, were performed with a JEOL JMS 5500 (SEM component) scanning electron microscopy (SEM). The elemental analysis was done with the EDAX Falcon spectrophotometer (Tokyo, Japan).

3. Results and discussion

3.1. Adsorption kinetics processes

3.1.1. Adsorption of the OII dye

The kinetics curves associated with the OII dye adsorption on the Chit-RH and the Chit-BN2 beads (Fig. 1a) showed similar trends, and the beads saturation was reached at the same time (~105 min) in spite of the clay minerals dissimilarity. Based on the values of the non-linear regression parameters (R^2, RMSE), and on the experimental and the calculated amounts of the OII dye retained at the equilibrium ($q_{e,exp}$, $q_{e,cal}$) (Table 4), the pseudo-first-order equation well-described the kinetics data of the dye adsorption on the Chit-RH beads. For the dye adsorption on the Chit-BN2 beads, the kinetics data fitted the pseudo-second-order equation, but given the closeness of the values of $q_{e,exp}$ and $q_{e,cal}$, the pseudo-first-order equation was also suitable.

The plots of the Boyd's equation (Fig. 2a) pointed out that up to 50 min the curves passed through the origin. So, the adsorption kinetics was limited by the intraparticle diffusion of the dye species [34]. The values of the diffusion coefficient (D), computed by using the following equation [30]: $D = BR_b^2/\pi^2$ (B is the slop of the curve $Bt = f(t)$, and R_b the radius of the bead (0.114 cm)) were found to be 4.1 × 10^{-11} and 3.4 × 10^{-11} m^2/s for the Chit-RH and the Chit-BN2 beads, respectively. Referring once again to Fig. 2a, the adsorption kinetics in the 65–90 min range was controlled by the dye transfer across the liquid film, as the intercepts did not go through the origin [34]. The mass transfer coefficients (k_e) calculated by using the mathematical expression [35]: $k_e = k_d(V/S)$ (k_d is determined from the plot of the equation $\ln(C_t/C_0) = -k_d t$ (Table 5); S is the surface of the beads (6.532 cm^2); V is the volume of the solution (200 cm^3)) were found to be 5.8 × 10^{-3} and 4.6 × 10^{-3} cm/s for the Chit-RH and the Chit-BN2 beads, respectively. Given these results, the transition from the intragranular diffusion to the transfer across the liquid film of the dye species took place in the span of 50–65 min. In addition, the mobility of the dye species was somewhat facilitated by using the stevensite-based beads.

3.1.2. Adsorption of the OG dye

The kinetics curves of the OG dye adsorption on the beads studied were similar in the 0–35 min span, and the equilibrium was achieved after 80 min (Fig. 1b). As supported by the results given in Table 4, the kinetics data followed well the pseudo-first-order equation. Based on the traces displayed in Fig. 2b, the adsorption rate at t < 15 min was controlled by the intraparticle diffusion of the dye species, and the coefficient of the diffusion was estimated to be 1.8 × 10^{-11} m^2/s. In the time interval of 20–50 min, the rate was chiefly controlled by the diffusion of the dye species across the liquid film. Considering the data given in Table 5, the transfer coefficients for the Chit-RH and the Chit-BN2 beads were found to be 2.88 × 10^{-3} and 3.28 × 10^{-3} cm/s, respectively. For t > 50 min, the kinetics was also controlled by the dye diffusion through the liquid film, but the transfer coefficients regressed (1.41 × 10^{-3} and 1.01 × 10^{-3} cm/s for the Chit-RH and the Chit-BN2 beads, respectively). The reduction of the transfer coefficients (50% for Chit-RH and 70% for Chit-BN2) was attributed to the thick liquid films built up around the particles, as it was supported by the increase of the absolute values of the intercepts of the curves $\ln(C_t/C_0) = f(t)$ (Table 5).

3.2. Adsorption isotherms and thermodynamic data

The isotherms of the OII and the OG dyes adsorption on both types of beads showed L shape (Fig. 3). So, the beads consisted of micropores, and the dyes species had a high affinity toward their active sites. Furthermore, both dyes seemed to be adsorbed without experiencing a strong competition from the solvent (water) molecules [36]. Based on the relative positions of the isotherms, it could be anticipated that the dyes adsorption took place endothermically.

The comparison of the fitting parameters (R^2 and RMSE) given in Table 6 allowed us to deduce that the adsorption isotherms fitted better by the model of D–R, and Langmuir's model was somewhat convenient. By contrast, the model of Freundlich was inappropriate. Bearing in mind the assumptions of the model of D–R, the adsorption process involved micropores, and occurred by pores filling. Moreover, it took place by physisorption as the energy (E) < 8 kJ/mol (Table 6).

The maximum adsorption capacity of the OII dye (Table 6) increased linearly with increasing temperature, and the estimated increments were 2.9 and 3.2 mg/g K for the Chit-RH and the Chit-BN2 beads, respectively. The maximum uptake of OG also increased with the rise of temperature, but the increase showed a parabolic trend.

Based on the calculated values of the Gibbs free energy change given in Table 7, the dyes adsorption on the Chit-RH and the Chit-BN2 beads occurred spontaneously,

Table 3
Planned experiments following the Doehlert design and their corresponding measured desorption deficiencies (*D*) of the dyes retained by the beads studied

Run	X_1	X_2	X_3	*I* (M)	pH	*T* (°C)	D(OII)%		D(OG)%	
							Chit-RH	Chit-BN2	Chit-RH	Chit-BN2
1	1.00	0.00	0.00	0.10	7	30	12.78	14.50	11.86	9.85
2	–1.00	0.00	0.00	0.00	7	30	12.78	14.40	9.66	7.13
3	0.60	1.00	0.00	0.08	9	30	19.36	18.67	14.44	13.56
4	–0.40	–1.00	0.00	0.03	5	30	12.78	13.21	5.40	3.54
5	0.60	–1.00	0.00	0.08	5	30	17.23	15.59	5.31	3.45
6	–0.40	1.00	0.00	0.03	9	30	19.36	17.48	13.09	12.11
7	0.60	0.50	0.80	0.08	8	38	18.78	16.78	12.90	9.18
8	–0.40	–0.50	–0.80	0.03	6	22	13.17	10.92	7.90	4.43
9	0.60	–0.50	–0.80	0.08	6	22	13.26	11.52	7.85	3.66
10	0.00	0.50	–0.80	0.05	8	22	13.46	16.09	11.50	6.66
11	–0.40	0.50	0.80	0.03	8	38	18.39	15.29	12.09	9.29
12	0.00	–0.50	0.80	0.05	6	38	13.17	16.88	9.89	5.03
13	0.00	0.00	0.00	0.05	7	30	12.88	14.10	12.41	9.60
14	0.00	0.00	0.00	0.05	7	30	12.88	14.10	12.41	9.45
15	0.00	0.00	0.00	0.05	7	30	12.88	14.10	12.48	9.60

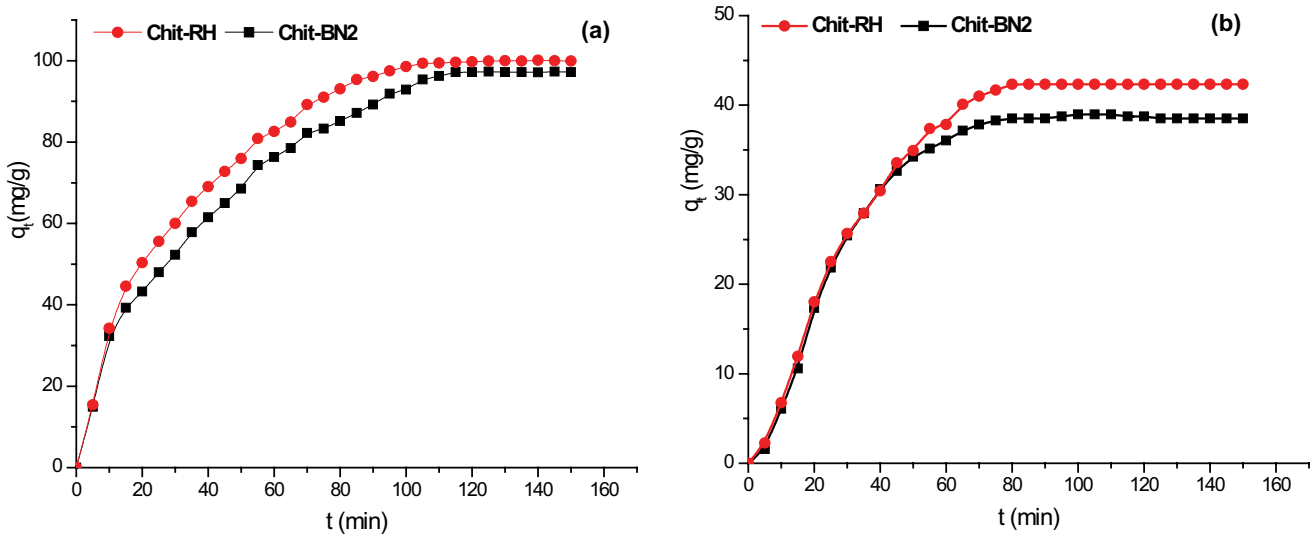

Fig. 1. Kinetics curves associated with the adsorption of the OII (a) and the OG (b) dyes on the Chit-RH and the Chit-BN2 beads.

and the chemical affinity of the OG species towards the beads sites was slightly high. Referring to the values of $\Delta H°$ (Table 7), the dyes adsorption was an endothermic process as previously expected, and it took place by physisorption ($\Delta H°$ < 40 kJ/mol). The retention of the dyes engendered an increase in the energy dispersion as the variation of the entropy was positive (Table 7).

3.3. Characterization of the dye-loaded beads

3.3.1. OII dye-loaded beads

The FT-IR analysis of the pristine and the OII dye-loaded Chit-RH beads showed that the dye adsorption resulted in a marked reduction of the intensity of the prominent band in the finger print region assigned to the Si–O stretch, and a slight intensification of the band at 627 cm^{-1} associated with the chitosan OH out-of-plane deformation (Fig. 4a). The deconvolution of the bands in the ranges of 3,750–3,000 cm^{-1} and 1,750–1,300 cm^{-1} (Fig. 5) pointed out that due to the retention of the dye: (i) the bands assigned to the stretching vibrations of the hydroxyls of the stevensite AlMgOH (3,672 cm^{-1}), and the chitosan (3,570 cm^{-1}) shifted slightly. (ii) the band associated with the stretching of the NH bond of the chitosan (3,371 cm^{-1}) appeared, and (iii) new bands, which were related to the deformation of the protonated amino-groups of the chitosan, occurred at

Table 4
Values of the parameters (k_1, k_2, and $q_{e,cal}$) of the pseudo-first-order and the pseudo-second-order kinetics equations, and their associated non-linear regression coefficients (R^2, RMSE)

Dyes		OII		OG	
Beads		Chit-RH	Chit-BN2	Chit-RH	Chit-BN2
Pseudo-first-order kinetics	k_1 (min^{-1})	0.032	0.028	0.020	0.022
	R^2	0.98	0.98	0.99	0.98
	RMSE	3.2	3.3	1.5	2.0
	$q_{e,cal}$ (mg/g)	100	96	54	49
Pseudo-second-order kinetics	k_2 (g/mg.min)	0.0002	0.0002	0.0002	0.0002
	R^2	0.99	0.99	0.99	0.98
	RMSE	3.8	2.4	1.6	2.2
	$q_{e,cal}$ (mg/g)	130	128	85	77
	$q_{e,exp}$ (mg/g)	100	97	50	46

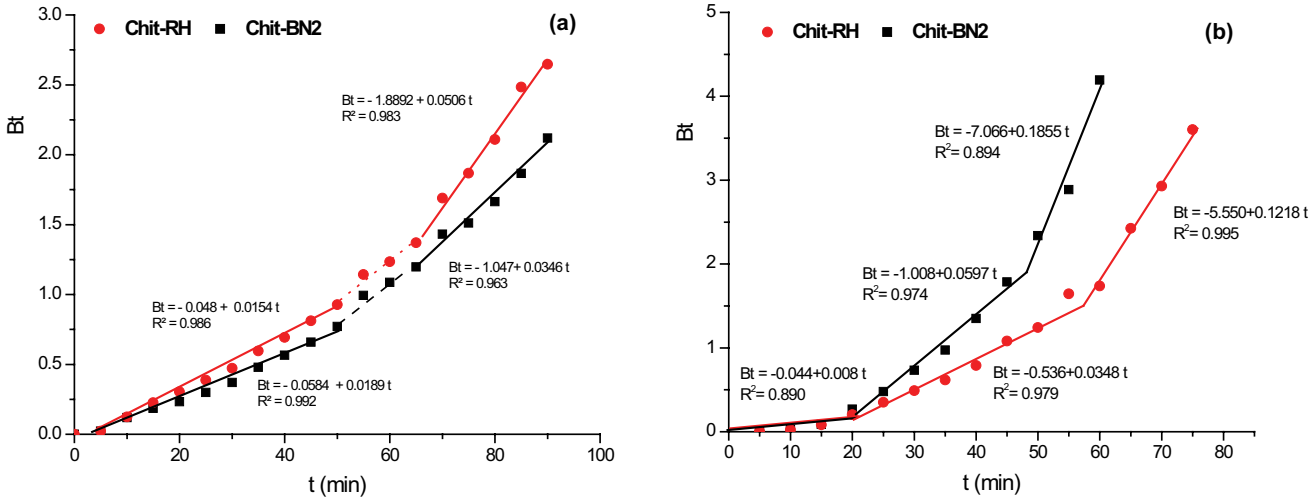

Fig. 2. Changes of the product *Bt* (*B*: Boyd's number, *t*: time) a function of time: (a) Orange II and (b) Orange G.

Table 5
Variations of $\ln(C_t/C_0)$ vs. time (t) related to the OII and the OG dyes adsorption on the beads studied

Time span (min)	Bead (Dye)	$\ln(C_t/C_0) = f(t)$
20–50	Chit-RH(OG)	–0.0057t–0.0528
	Chit-BN2(OG)	–0.0065t–0.0261
60–75	Chit-RH(OG)	–0.0029t–0.1912
	Chit-BN2(OG)	–0.0020t–0.2198
65–90	Chit-RH(OII)	–0.0114t–0.4550
	Chit-BN2(OII)	–0.0090t–0.4286

1,532 and 1,515 cm^{-1}. These results allowed us to infer that the dye retention implicated the amino-groups of the chitosan. Also, the octahedral sheets of the stevensite were directly or indirectly involved.

The SEM examinations, specifically the energy-dispersive X-ray spectroscopy (EDS) analysis, supported the dye retention since the peak of the sulfur, which is a chemical constituent of the sulfonate of the OII dye, was revealed (Fig. 6b). The examinations also showed that the alike-squamates at the surfaces of the pristine Chit-RH beads (Fig. 6a) partially vanished and the feature of the surface slightly changes as the dye was adsorbed (Fig. 6b). Comments regarding this change will be given later.

As shown in Fig. 4b, the FT-IR bands lying in the functional group region became discernible on the spectrum of the OII dye-loaded Chit-BN2 beads. So, the environment of the hydroxyls of the chitosan and of the clay particles was altered. The modification of the environment of the chitosan hydroxyls was supported by the alteration of the intensity of the band at 616 cm^{-1} assigned to the OH out-of-plane deformation. The deconvolution of the bands in the 1,800–1,300 cm^{-1} region (Fig. 7) indicated that the positions of the bands associated with the vibrations of C=O (1,690 cm^{-1}), NH_3^+ (1,556 cm^{-1}), and CH (1,433 and 1,386 cm^{-1}) were not affected as a result of the dye adsorption. However, the band at 1,467 cm^{-1} attributed to the methylene C–H bend vanished. In this respect, it should be noted that the CH_2 group positioned at the C-6 of the pyranose

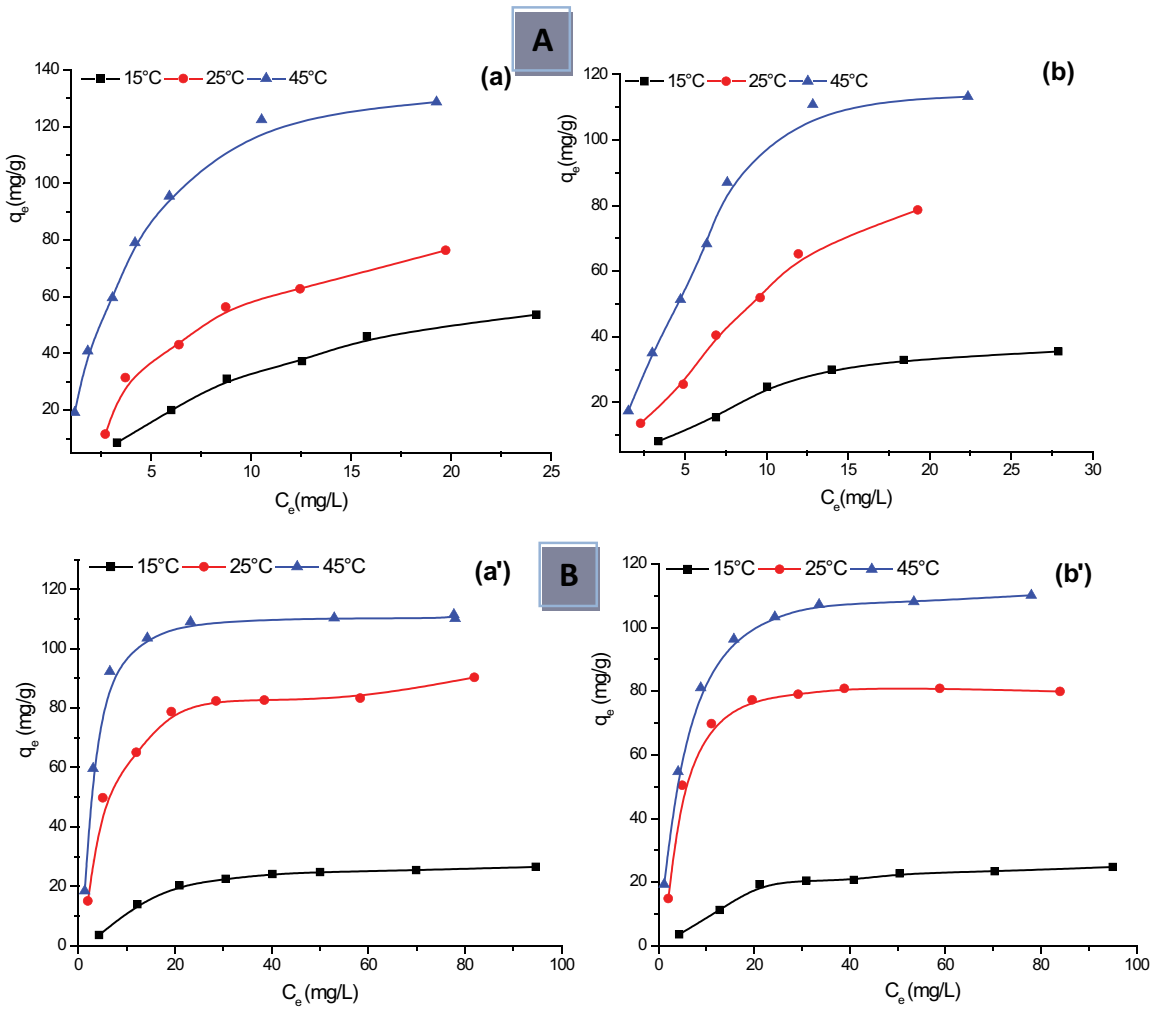

Fig. 3. Equilibrium isotherms of the OII (A) and the OG (B) dyes adsorption on the Chit-RH (a and a′) and the Chit-BN2 (b and b′) beads.

Table 6
Values of the parameters of the isotherms models used and the non-linear regression coefficients

	Dyes	OII						OG					
	Beads	Chit-RH			Chit-BN2			Chit-RH			Chit-BN2		
	T (K)	288	298	318	288	298	318	288	298	318	288	298	318
Langmuir's model	q_m (mg/g)	87	116	175	52	135	175	32	97	120	30	90	120
	K_L (L/mg)	0.058	0.090	0.178	0.079	0.063	0.102	0.064	0.172	0.310	0.058	0.217	0.220
	R^2	0.96	0.96	0.98	0.95	0.97	0.95	0.96	0.97	0.94	0.95	0.94	0.99
	RMSE	4.1	5.9	7.8	2.7	5.5	9.2	1.8	5.2	9.1	1.7	6.7	3.2
Freundlich's model	K_F ($mg^{1-1/n}L^n/g$)	8.69	16.16	36.22	7.62	13.37	24.59	5.78	30.30	49.67	4.90	35.19	41.2
	$1/n$	0.54	0.50	0.46	0.46	0.57	0.53	0.35	0.27	0.20	0.37	0.23	0.25
	R^2	0.89	0.89	0.89	0.87	0.92	0.88	0.83	0.82	0.71	0.84	0.72	0.84
	RMSE	6.2	8.9	14.9	4.3	8.4	13.9	3.5	11.7	19.5	3.1	13.5	14.2
D–R model	q_m (mg/g)	71	99	157	46	108	148	30	93	118	27	88	116
	E (kJ/mol)	0.85	1.05	1.47	0.91	0.93	1.20	0.78	1.25	1.66	0.75	1.33	1.49
	R^2	0.99	0.98	0.99	0.98	0.98	0.97	0.99	0.98	0.97	0.98	0.97	0.99
	RMSE	2.1	3.8	3.8	1.7	4.1	6.8	0.6	3.2	8.4	1.2	4.5	2.3

Table 7
Thermodynamic data associated with the OII and the OG dyes adsorption on the Chit-RH and the Chit-BN2 beads

Dyes	OII						OG					
Beads	Chit-RH			Chit-BN2			Chit-RH			Chit-BN2		
T (K)	288	298	318	288	298	318	288	298	318	288	298	318
$\Delta G°$ (kJ/mol)	–33.37	–35.63	–39.81	–34.11	–34.75	–38.34	–34.23	–37.85	–41.95	–33.94	–39.01	–41.03
$\Delta H°$ (kJ/mol)		28.24			7.96			37.87			28.98	
$\Delta S°$ (kJ/K mol)		0.19			0.14			0.23			0.20	

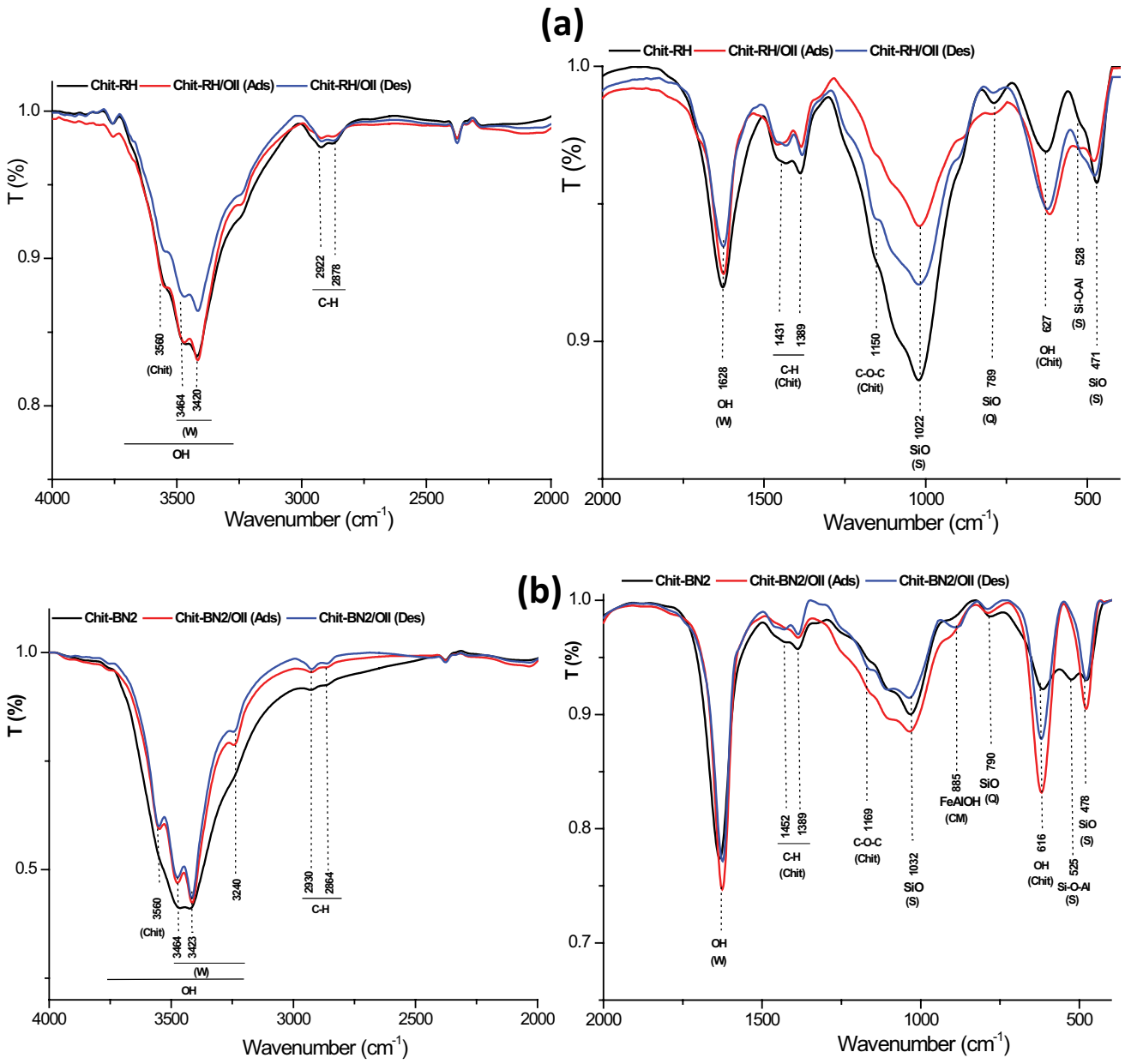

Fig. 4. FT-IR spectra of the pristine beads, the OII dye-loaded beads (Chit-RH/OII (Ads), Chit-BN2/OII (Ads)), and the dye-unloaded beads (Chit-RH/OII (Des), Chit-BN2/OII (Des)). (a) Chit-RH and (b) Chit-BN2. Chit: chitosan, W: water, S: silicates, Q: quartz, CM: clay minerals.

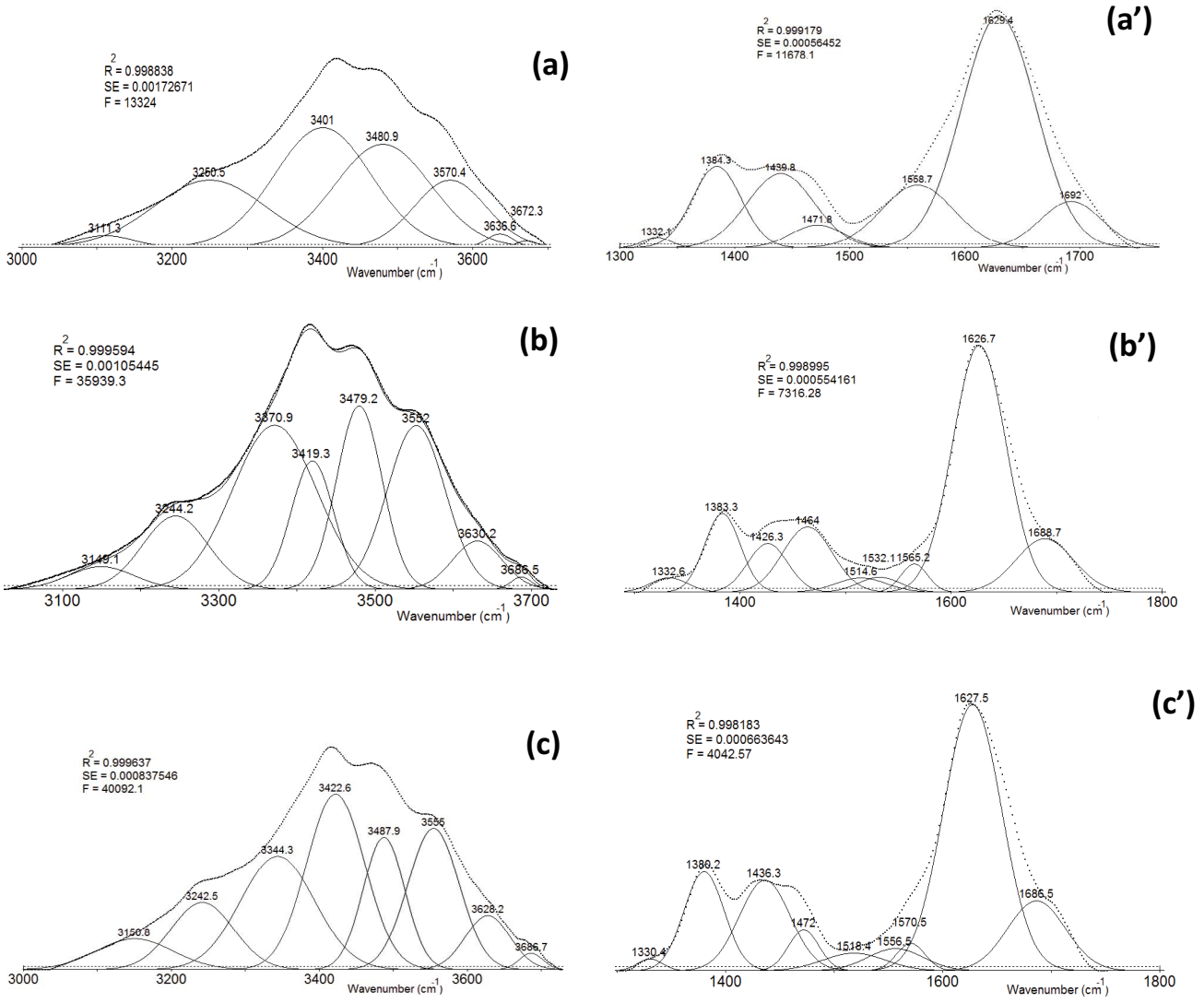

Fig. 5. Deconvoluted bands of the FT-IR spectra of the pristine beads (a and a'), the OII dye-loaded beads (b and b'), and the dye-unloaded beads (c and c').

ring is linked to the hydroxyl, which is considered to be a reactive group [37]. In the light of these results, the OII dye retention by the Chit-BN2 beads involved particularly the hydroxyls of the C-6 groups of the chitosan chains.

3.3.2. OG dye-loaded beads

By reference to the FT-IR spectrum of the Chit-RH pristine beads, the spectrum of the OG loaded-beads displayed extra faint bands at 1,544 and 1,325 cm^{-1} (Fig. 8a) assigned to the vibrations of the azo and the C–N bonds of the azo dye adsorbed, respectively [38]. In addition, the shapes of the bands attributed to the CH (1,431 and 1,389 cm^{-1}) and the OH out-of-plane deformation of the chitosan (627 cm^{-1}) were somewhat altered. These facts were taken as a sign of the implication of the chitosan in the dye adsorption.

A comparative examination of the FT-IR spectra of the Chit-BN2 beads taken before and after the adsorption of the OG dye (Fig. 8b) pointed out that in the contact with the dye the stretching vibrations of the OH bonds of the chitosan (3,560 cm^{-1}) and the water retained (3,464; 3,423; and 3,240 cm^{-1}) were well-differentiated. Such a split of the band in the 3,700–3,000 cm^{-1} range also occurred in the case of the adsorption of the OII dye by the Chit-BN2 beads, and the mechanism behind this fact was linked to the change of the environment of the hydroxyl groups. The spectrum of the OG dye loaded Chit-BN2 beads displayed faint bands related to the azo bond vibration (1,550 cm^{-1}) and to the C–N stretching vibration (1,320 cm^{-1}). In addition, the intensities of the bands associated with the CH and the OH bonds of the chitosan changed as a result of the OG dye adsorption. Considering the latter observation, together with the results given above, the chitosan was the active component in the OG dye retention by the Chit-BN2 beads.

3.4. Release of the dyes by the dye-loaded beads

3.4.1. Effects of the operating factors on the desorption efficiency

The statistical results given in Table 8 showed that: (i) the Fisher-ratio (*F*) largely exceeded unity, (ii) the correlation

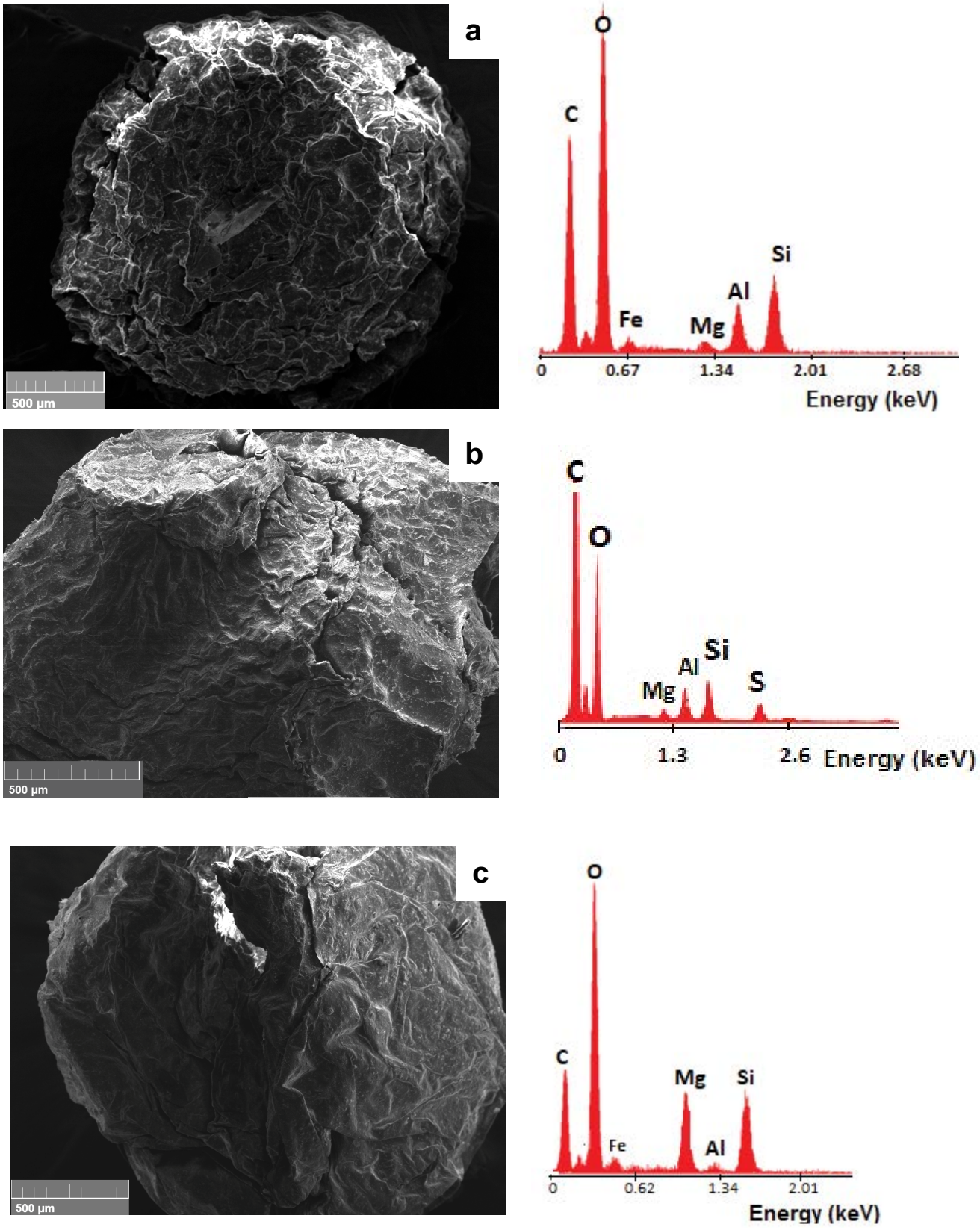

Fig. 6. SEM micrographs and the EDS spectra of the Chit-RH beads: (a) pristine, (b) OII dye-loaded, and (c) OII dye-unloaded.

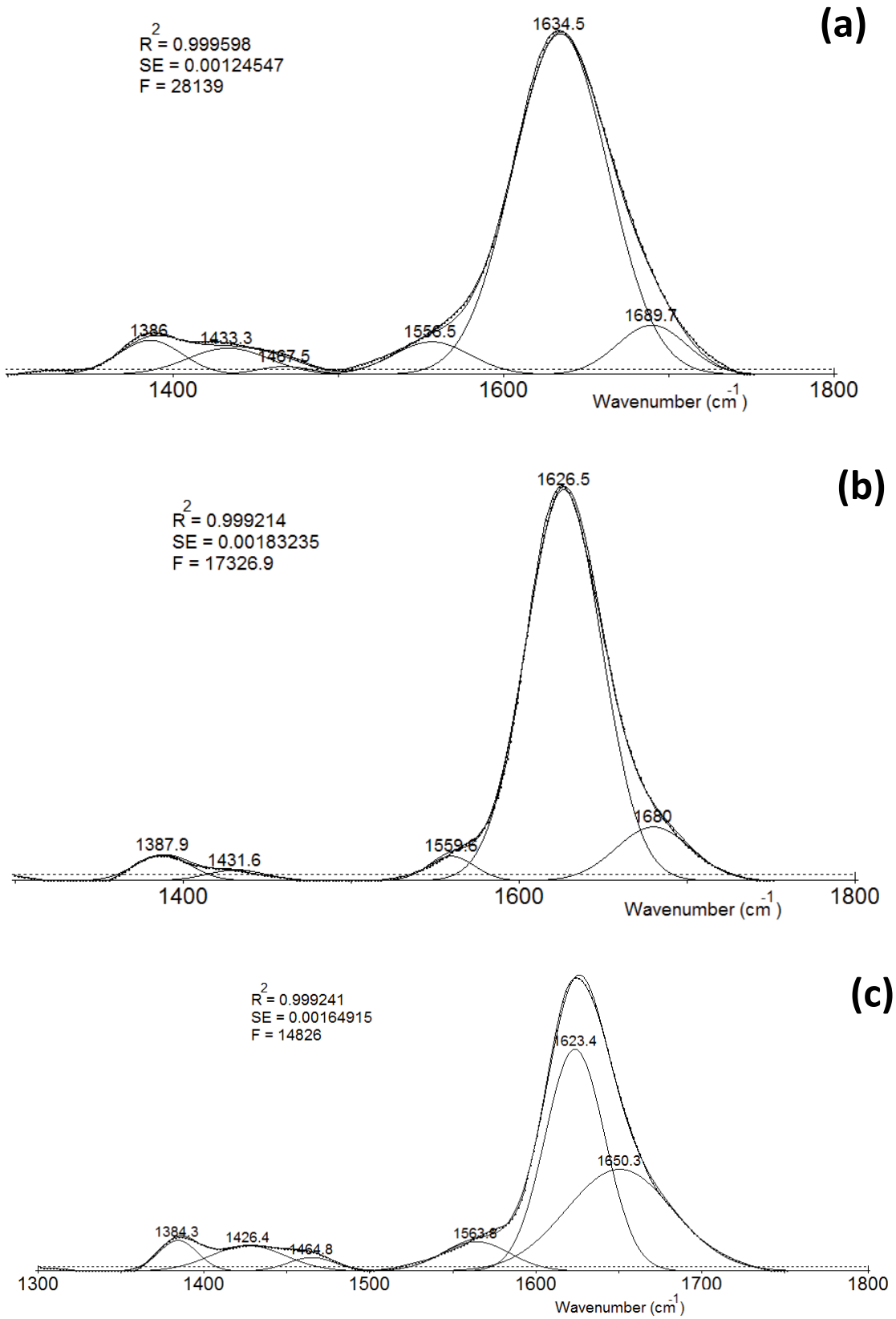

Fig. 7. Deconvoluted bands in the 1,800–1,300 cm^{-1} region of the FT-IR spectra of the beads: (a) pristine, (b) OII dye-loaded, and (c) OII dye-unloaded.

coefficient (R^2) approximated 1, and (iii) the probability (P) of obtaining a ratio of mean squares was below 0.01. Therefore, the changes of the desorption efficiency of the OII dye (D(Chit-RH/OII), D(Chit-BN2/OII)) and the OG dye (D(Chit-RH/OG), D(Chit-BN2/OG)) retained by the beads studied vs. the ionic strength, the pH, and the temperature followed well the equations:

$$D(\text{Chit-RH/OII}) = 12.79 + 0.606X_1 + 2.506X_2 + 1.63X_3 + 0.102X_1^2 + 4.296X_2^2 + 1.079X_3^2 - 2.266X_1X_2 + 1.654X_1X_3 + 3.122X_2X_3 \quad (5)$$

$$D(\text{Chit-BN2/OII}) = 14.016 + 0.677X_1 + 1.915X_2 + 1.734X_3 + 0.559X_1^2 + 2.008X_2^2 + 0.674X_3^2 - 0.602X_1X_2 + 0.941X_1X_3 - 3.838X_2X_3 \quad (6)$$

$$D(\text{Chit-RH/OG}) = 12.43 + 0.802X_1 + 4.541X_2 + 1.557X_3 - 1.673X_1^2 - 3.273X_2^2 - 1.881X_3^2 + 0.831X_1X_2 + 0.233X_1X_3 - 1.287X_2X_3 \quad (7)$$

$$D(\text{Chit-BN2/OG}) = 9.55 + 0.740X_1 + 5.029X_2 + 1.786X_3 - 1.06X_1^2 - 1.493X_2^2 - 4.124X_3^2 + 0.889X_1X_2 + 0.09X_1X_3 + 0.971X_2X_3 \quad (8)$$

The comparison of the magnitudes of the linear terms of these equations allowed us to deduce that the increase of the value of any factor among the studied ones favored the dyes desorption, and the weights of their effects followed this order: pH > T > I. Considering the pH_{PZC} given in Table 1, the positive effect of the increase of the pH on the release of the dyes could be associated with the increase of the density of the negative charges of the beads. Indeed, based on the pKa of the chitosan (~6.5), the $-NH_2$ moieties of the chitosan should increase at the expense of the protonated amino-group ($-NH_3^+$) with the increase of pH. In such a condition, the adsorption sites were annihilated, and the dye species retained should be desorbed. In addition to the latter fact, the increase of the pH also engendered an increase of the density of the negative charges of the dyes, especially as the pH exceeded the pH_{PZC} (Table 1).

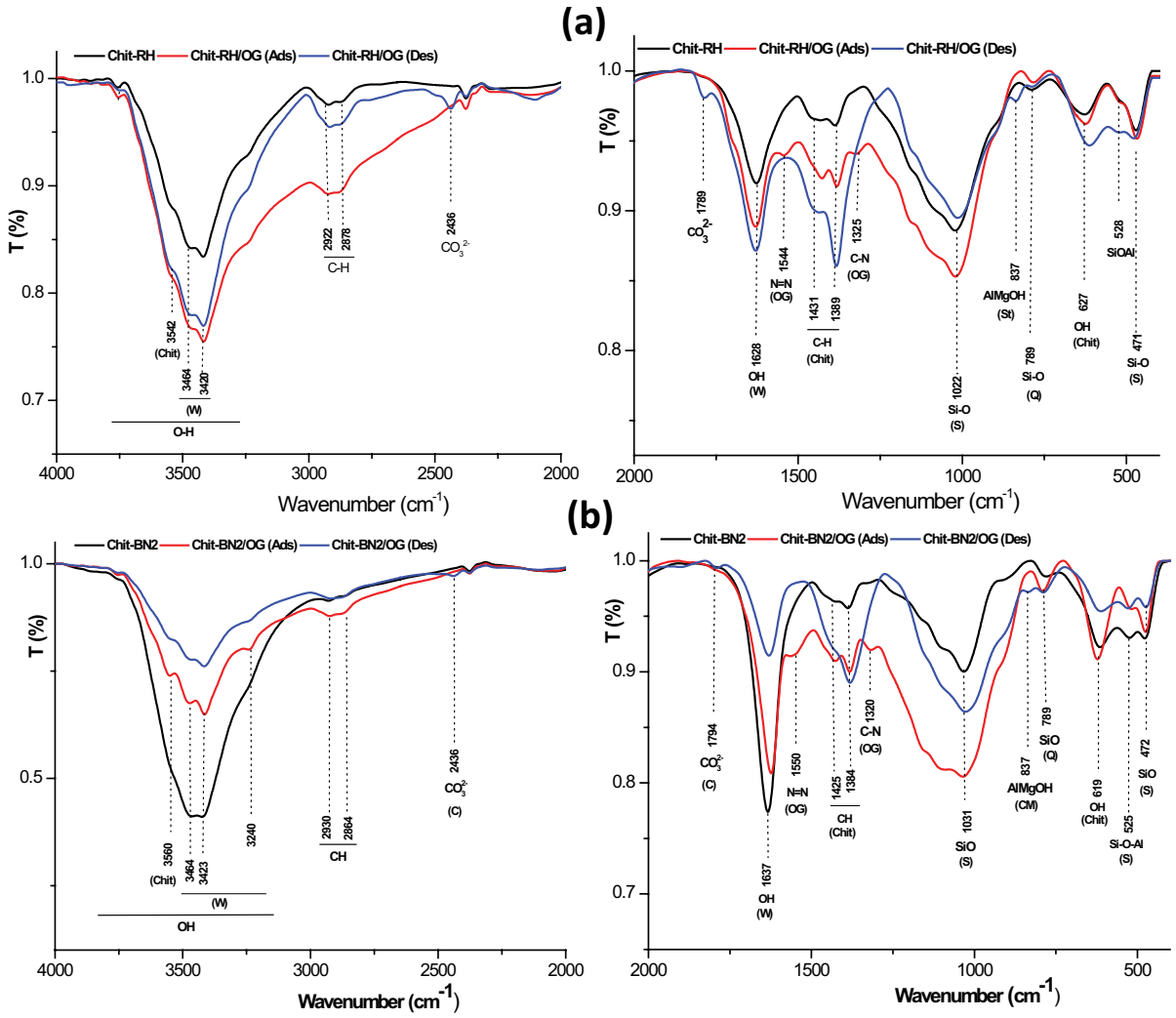

Fig. 8. FT-IR spectra of the pristine beads, the OG dye-loaded beads (Chit-RH/OG (Ads), Chit-BN2/OG (Ads)), and the dye-unloaded beads (Chit-RH/OG (Des), Chit-BN2/OG (Des)). (a) Chit-RH and (b) Chit-BN2. Chit: chitosan, W: water, S: silicates, Q: quartz, CM: clay minerals.

Table 8
ANOVA results and the fitting coefficient values associated with the polynomial models adopted

		Sources of variation	Sum of squares	Degrees of freedom	Mean squares	*F*-ratio	Signification	R^2
Chit-RH	OII	Regression	105.2552	9	11.6950	15.9894	0.486**	0.966
		Residues	3.6571	5	0.7314			
		Total	108.9123	14				
	OG	Regression	110.6253	9	12.2917	7,525.5273	<0.01***	0.986
		Residues	1.5766	5	0.3153			
		Total	112.2019	14				
Chit-BN2	OII	Regression	60.9165	9	6.7685	17.7962	0.397***	0.970
		Residues	1.9017	5	0.3803			
		Total	62.8182	14				
	OG	Regression	140.4897	9	15.6100	2,081.3288	<0.01***	0.974
		Residues	3.7674	5	0.7535			
		Total	144.2571	14				

The eventual increase of the amount of the dyes desorbed due to the temperature rise expressed the presence of weak bonds between the dye species and the active sites of the beads. Such bonds were dissociated as the ionic strength of the solution increased. It was believed that in the latter case, thick hydrated atmospheres composed of Na^+ and Cl^- ions (the NaCl electrolyte derivatives) developed around the dyes species on one hand, and the active sites of the beads on the other hand; thereby the attractive forces between the dyes species and the beads should be reduced.

The comparison of the absolute values of the coefficients a_{ij} suggested that the most important interaction between the factors was the one that exists between pH and *T*. Considering the algebraic values, the simultaneous increase of pH and *T* resulted in an increase in the release of the OII dye by the Chit-RH beads, and the orange G by the Chit-BN2 beads. In contrast, the release of the OII dye by the Chit-BN2 beads or the OII dye by the Chit-RH beads was impeded. As far as the interaction between the factors was considered, the ionic strength and the pH manifested antagonistic interaction in the case of the release of the OII dye by both types of beads. However, the factors interacted synergistically in the case of the OG dye desorption. The interaction between the ionic strength and the temperature was synergetic for both the dyes and the beads used.

3.4.2. Determination of the optimum operating conditions for the dyes release

The determination study of the desirable set of the operating factors for the optimum efficiency of the desorption of both dyes by the beads studied showed that the suitable combination should be as follows: I = 0.08 M, pH = 8, and T = 36°C. The optimum desorption efficiencies at 2 h, calculated and measured in the latter operating conditions, are given in Table 9. The closeness of the values of D_{cal} and D_{mes} was an additional support for the validity of the aforementioned models.

Table 9
Optimum desorption efficiencies measured (D_{mes}) and calculated (D_{cal}) in the operating conditions (I = 0.08 M, pH = 8, and T = 36°C) determined by using the response surface methodology and the desirability function approach

Dyes	Beads	D_{cal}(%)	D_{mes}(%)
OII	Chit-RH	19.9	19.6
	Chit-BN2	18.7	18.7
OG	Chit-RH	14.2	14.3
	Chit-BN2	13.8	13.6

3.4.3. Time effect on the dyes desorption and the reuse ability of the beads

The variations of the desorption efficiency of the OII and the OG dyes vs. time showed similar trends (Fig. 9), and the mathematical relations were as follows:

$$\frac{D}{D_{max}}(\text{OII dye}) = 0.97\exp\left(-\exp\left(-1.2 \pm 0.1(t-2.4)\right)\right) \quad (9)$$

$$\frac{D}{D_{max}}(\text{OG dye}) = 1.00\exp\left(-\exp\left(-1.65 \pm 0.05(t-2.4)\right)\right) \quad (10)$$

This result indicated that the rate constant (1.2 min^{-1}) associated with the release of the OII dye was independent of the nature of the beads used. The same was observed for the rate constant (1.65 min^{-1}) associated with the desorption of the OG dye. So, the contribution of the clay minerals in the dyes retention by the beads was insignificant, as previously reported.

As can be deduced from Fig. 10, the beads studied could be reused as adsorbents for both dyes, but their maximum adsorption capacities regressed significantly after the third cycle. In addition, the adsorption efficiency of the Chit-RH beads was relatively high, and it remained acceptable after

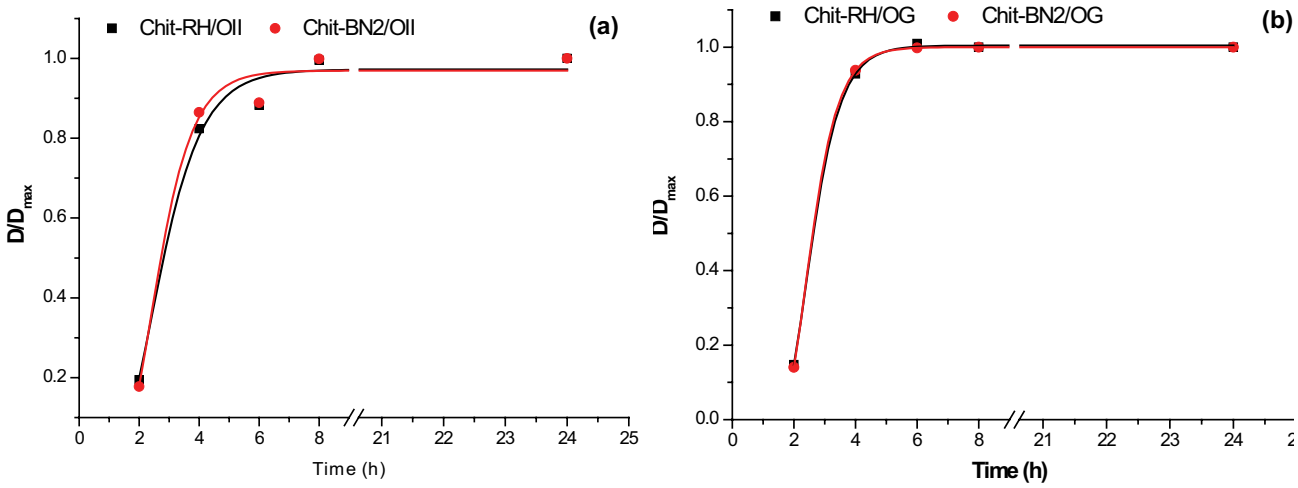

Fig. 9. Variations of the desorption efficiency (*D*) of the OII (a) and the OG (b) dyes against time.

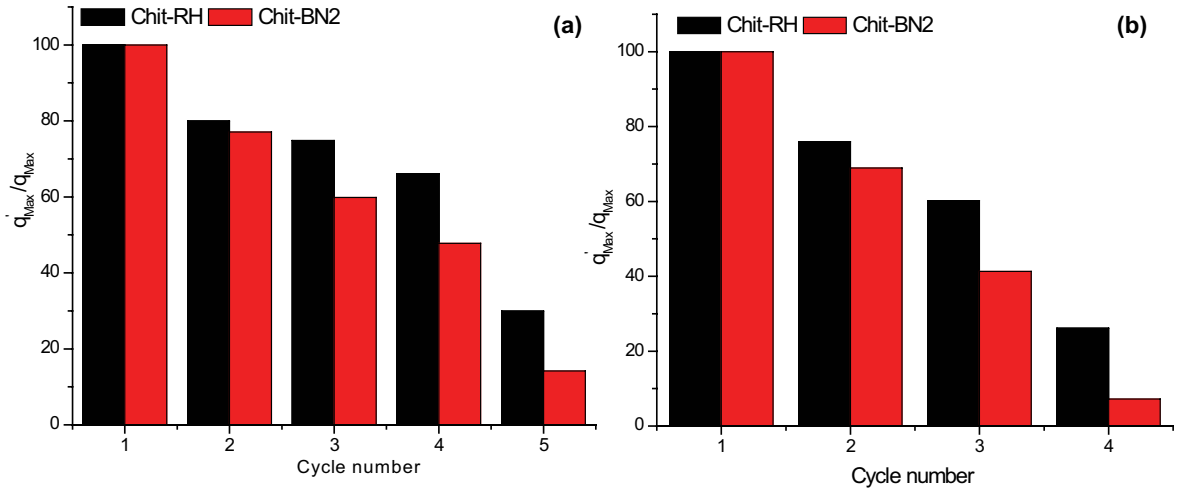

Fig. 10. Evolutions of the maximum amounts of the OII (a) and the OG (b) dyes retained by the beads studied vs. the adsorption–desorption cycle number.

the fourth adsorption–desorption cycle. Based on these data it was believed that due to the successive adsorption–desorption cycles, the chains of the chitosan placed at the beads surfaces were gradually detached, but those which were tightly bound to the clay particles, such as the chains within the interlayer space of the stevensite, kept their adsorption activity.

3.4.4. Characterization of the regenerated beads and adsorption mechanisms

The FT-IR spectrum of the OII dye-unloaded Chit-RH beads did not show a noticeable change in the positions of the main bands observed on the other spectra given in Fig. 4a. However, recalling the plots in Fig. 5, the bands linked to the stretching of the NH bond (3,344 cm^{-1}) and to the deformation of the protonated amine (1,556 cm^{-1}) shifted as the OII dye was removed. This observation supported the fact that the amino-groups of the chitosan were the most important sites involved in the OII dye retention process. The SEM examinations revealed a marked change in the feature of the surface of the unloaded beads (Fig. 6). The somewhat smooth and wavy surfaces of the unloaded beads together with the FT-IR results given above allowed us to deduce that in the contact with the OII dye species the entangled chains of the chitosan became undone, and some of them were released together with the dye species.

The FT-IR spectra of the OII dye-loaded and the unloaded Chit-BN2 beads were similar (Fig. 4b); so the dye release did not disturb the interactions between the chitosan chains. On the other hand, the microscopic observations of the unloaded beads showed that the aspect of their surfaces resembled that shown in Fig. 6c, but the beads presented marked failures, presumably because of the local scarcity of the chitosan, known as a film-forming material.

The FT-IR analysis of the OG dye-loaded and the unloaded beads of the Chit-RH and the Chit-BN2 composites indicated that the spectra of the unloaded beads

consisted of faint bands at 2,436 and 1,794 or 1,789 cm^{-1} (Fig. 8). These unexpected bands were assigned to the Na-carbonate (Na_2CO_3) formed as a result of the reaction between the carbon dioxide of the atmosphere and the Na^+ ions (OG dye derivatives). Such a reaction of carbonation also occurred in different experimental conditions [32]. Considering the deconvolution plots shown in Fig. 11, the shapes of the bands attributed to the CH_3 (1,381.6 and 1,382.4 cm^{-1}) and the CH_2 (1,456.7 and 1,452.3 cm^{-1}) belonging to the $NHCOCH_3$ and CH_2OH groups were markedly altered as the OG dye was released. In addition, the band associated with the stretching vibration of the C=O bond in the $NHCOCH_3$ (1,701.4 cm^{-1}) changed, especially in the case of the Chit-RH beads (Figs. 11a and b). For the Chit-BN2 beads, this band shifted from 1,663.3 to 1,679.9 cm^{-1} (Figs. 11a and b). In light of these results, the CH_2OH and the $NHCOCH_3$ groups of the chitosan were involved in the adsorption of the OG dye species on the Chit-RH and the Chit-BN2 beads.

At the operating pH (4.5), the surfaces of the Chit-RH and the Chit-BN2 beads were almost neutral because the pH was close to the pH_{PZC} (Table 1). In addition, the basic forms of the dyes studied were almost negligible ([base]/[acid] = 1.3×10^{-7} for the OII dye, and 5×10^{-9} for the OG dye). In such a condition, the acid forms of the OII and the OG dyes were the species adsorbed, and the sulfonic acid functional groups were the main active part of the dyes species. The sulfonic groups of the dyes were attached to the chitosan by weak bonds involving the protonated amine (NH_3^+), the CH_2OH, and/or the $NHCOCH_3$ groups. A schematic representation of the mechanisms of the OII and the OG dyes adsorption on the beads studied is given in Fig. 12.

Considering the characteristics of the chitosan used (MW = 53,819 g/mol; DD = 90%) and the weight of the glucosamine units, which were estimated to be 300/mol, the amount of the amino-group per gram of beads was determined to be 2.8×10^{-3} mol. Taking, for instance, the weight of the Chit-RH beads utilized in the adsorption test, and the CEC of the basic clay (0.8 meq/g) [23], the amount of the active sites of RH was calculated to be 0.4×10^{-3} mol/g of beads. Thus, the amount of the amino-groups of the

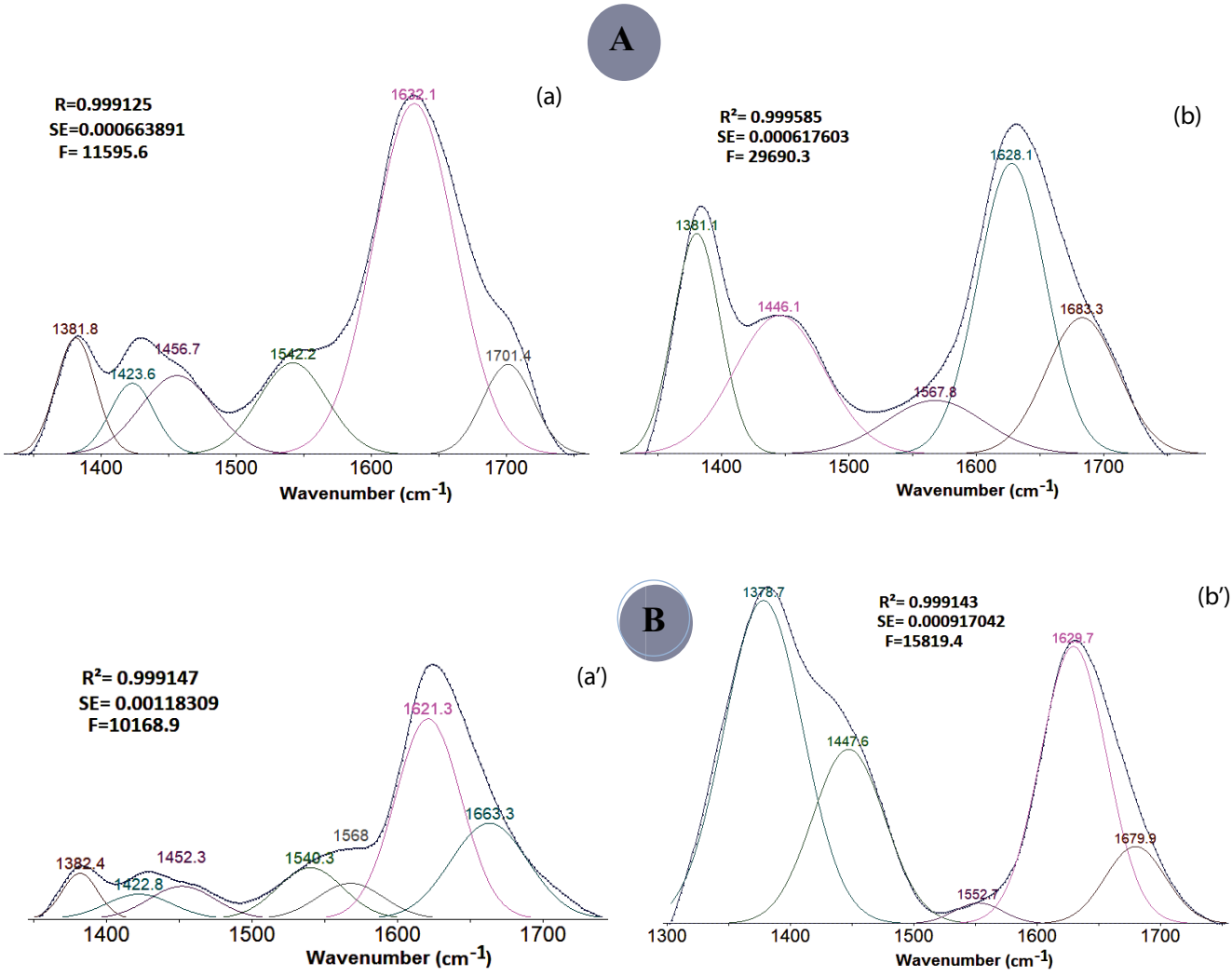

Fig. 11. Deconvoluted bands in the 1,800–1,300 cm^{-1} region of the FT-IR spectra of the OG dye-loaded (a and a′) and the unloaded beads (b and b′). (A) Chit-RH beads and (B) Chit-BN2 beads.

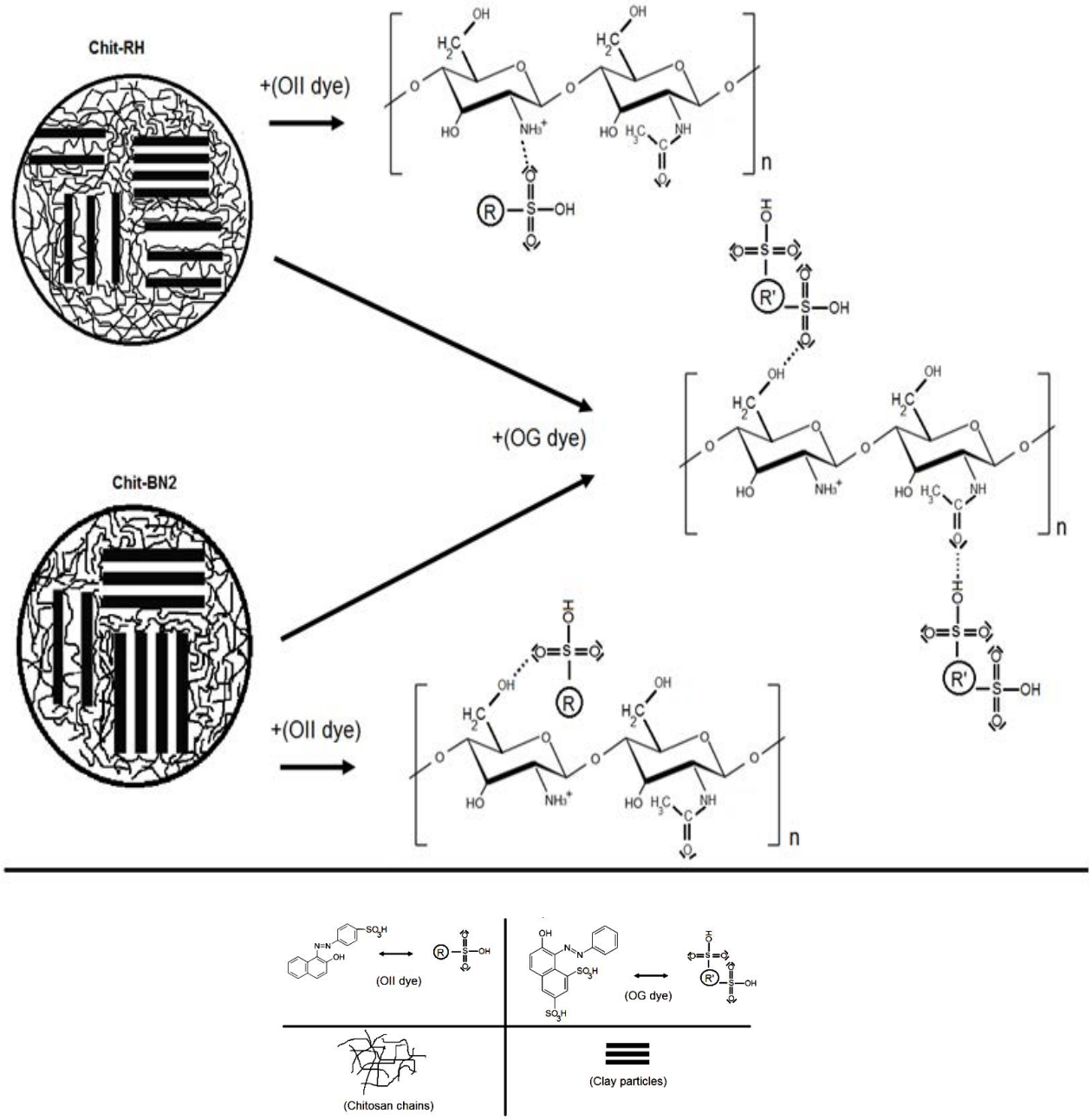

Fig. 12. Schematic representation of the mechanisms of the OII and the OG dyes adsorption on the beads studied.

chitosan, considered to be the active sites of the biopolymer, exceeded that of the clay, and the beads were formed of bundles of polymer chains. Considering, for instance, the values of q_m associated with the adsorption of the OII on the Chit-RH beads (Table 6), the eventual quantity of the OII dye retained would be 7, 10, and 16 mol% at 15°C, 25°C, and 45°C. Therefore, only a small portion of the active sites of the biopolymer was involved in the adsorption process. The main fraction of the chitosan was implicated in the chain linkage on the one hand, and the formation of bounds with the clay particles, on the other hand.

Compared to the organoclays listed in Table 10, the beads studied showed higher adsorption capacities of OII. However, the maximum uptakes of OG were smaller than those of the surfactant-composed organoclays, but they remained high in comparison with that of the modified chitosan beads (Table 10).

4. Conclusion

The results of this study led to the following conclusions: (i) the saturation time (≤105 min) for both beads was not affected by the clay mineralogy as the clay particles

Table 10
Maximum amounts of the OII and the OG dyes retained by the beads studied and by different adsorbents

Adsorbent	q_m (mg/g)		References
	OII	OG	
ODTMA-modified palygorskite	88		[39]
DODMA-modified palygorskite	92		
Surfactant-modified montmorillonite			
–CPC–MMT		136.986	[40]
–CTAB–MMT		126.582	
Organoclay (HDTMA-Bentonite)	11.15		[41]
Surfactant-coated zeolite	38.96		[42]
Zirconium-based chitosan microcomposite	926		[43]
Surfactant-modified montmorillonite			
–B–NHTPB	53.78		[44]
–B–MTPB	33.79		
Chitosan-diatomite membrane		588	[45]
Polyaniline/bentonite nanocomposite	105.9		[18]
Modified chitosan beads		63.67	[46]
Chit-RH	116	97	This study
Chit-BN2	135	90	This study

were wrapped with the chitosan chains, (ii) at the early stage of the dyes adsorption, the intraparticle diffusion was the main rate-controlling step of the processes. However, at long adsorption times, the transfer across the liquid film was the rate-limiting step. The coefficients of the diffusion and of the mass transfer of the OII dye were approximately two-fold higher than those of the OG dye, (iii) the equilibrium adsorption isotherms fitted well the D–R model, and the maximum amounts of the OII and the OG dyes retained at 298 K were in the ranges of 115–136 mg/g and 89–98 mg/g, respectively, (iv) the weights of the effects of the operating factors on the desorption efficiency were well assessed by using the RSM. The weights of the effects followed this order: pH > T > I, and the most influential interaction was that between pH and T, (v) both beads were regenerated, and their adsorption abilities in the third cycle were in the range of 40%–75%. The higher adsorption abilities were those of the regenerated stevensite-based beads, and (vi) the chitosan was the active constituent of the beads as the azo dyes species were retained by the protonated amino-groups (NH_3^+), the hydroxyls, and the $NHCOCH_3$ moieties.

Acknowledgments

This study was financially supported by the CNRST (Morocco) under grant (PPR/26/2015).

Symbols

B — Boyd's number
B — Constant, $(mol/J)^2$
C_r — Concentration of the dye released at 2 h in the solution, mg/L
C_e — Concentration of the dye at equilibrium, mg/L
C_0 — Initial concentration of the dye, mg/L
C_t — Instantaneous concentration of the dye, mg/L
E — Mean energy of adsorption, J/mol
ε — Polanyi potential
$\Delta G°$ — Gibbs free energy change, J/mol
$\Delta H°$ — Heat change, J/mol
I — Ionic strength, M
k_1 — First-order rate constant, min^{-1}
k_2 — Second-order rate constant, g/mg min
K_F — Constant of Freundlich, $(mg/g)(L/mg)^{1/n}$
K_L — Constant of Langmuir, L/mg
K_c — Equilibrium constant
m — Dose of the beads, g
M_w — Molecular weight of the adsorbate, g/mol
n — Number of trials performed
$\bar{q}_m$ — Average of the values of q_m
q_d — Amount of the dye released in the solution, mg/g
q_e — Equilibrium retained amount, mg/g
q_t — Instantaneous retained amount, mg/g
q_{max} — Maximum uptake of the dye, mg/g
q_m — Measured amount of the dye retained
q_c — Calculated amount of the dye retained
R — Gas constant, 8.31 J/K mol
$\Delta S°$ — Entropy change, J/K mol
T — Temperature
t — Time
V — Volume of the solution, L

References

[1] R.W. Sabnis, Handbook of Biological Dyes and Stains – Synthesis and Industrial Applications, John Wiley & Sons, Inc., Hoboken, NJ, 2010.

[2] R.G. Saratale, G.D. Saratale, J.S. Chang, S.P. Govindwar, Bacterial decolorization and degradation of azo dyes: a review, J. Taiwan Inst. Chem. Eng., 42 (2011) 138–157.
[3] E. Forgacs, T. Cserhati, G. Oros, Removal of synthetic dyes from wastewaters: a review, Environ. Int., 30 (2004) 953–971.
[4] A. Pandey, P. Singh, L. Iyengar, Bacterial decolorization and degradation of azo dyes, Int. Biodeterior. Biodegrad., 59 (2007) 73–84.
[5] A. Bafana, S.S. Devi, T. Chakrabarti, Azo dyes: past, present and the future, Environ. Rev., 19 (2011) 350–370.
[6] T. Robinson, G. McMullan, R. Marchant, P. Nigam, Remediation of dyes in textile effluent: a critical review on current treatment technologies with a proposed alternative, Bioresour. Technol., 77 (2001) 247–255.
[7] A. Kausar, M. Iqbal, A. Javed, K. Aftab, Z.-i.-H. Nazli, H.N. Bhatti, S. Nouren, Dyes adsorption using clay and modified clay: a review, J. Mol. Liq., 256 (2018) 395–407.
[8] C.F. Mok, Y.C. Ching, F. Muhamad, N.A. Abu Osman, N.D. Hai, C.R. Che Hassan, Adsorption of dyes using Poly(vinyl alcohol) (PVA) and PVA-based polymer composite adsorbents: a review, J. Polym. Environ., 28 (2020) 775–793.
[9] H. Murray, Applied Clay Mineralogy: Occurrences, Processing and Applications of Kaolins, Bentonites, Palygorskite, Sepiolite, and Common Clays, Elsevier Ltd., Netherlands, 2007.
[10] B.K. Bozoğlan, O. Duman, S. Tunç, Preparation and characterization of thermosensitive chitosan/carboxymethylcellulose/scleroglucan nanocomposite hydrogels, Int. J. Biol. Macromol., 162 (2020) 781–797.
[11] L. Wang, A. Wang, Adsorption behaviors of Congo red on the *N*,*O*-carboxymethyl-chitosan/montmorillonite nanocomposites, Chem. Eng. J., 143 (2008) 43–50.
[12] S. Kittinaovarat, P. Kansomwan, N. Jiratumnukul, Chitosan/modified montmorillonite beads and adsorption Reactive Red 120, Appl. Clay Sci., 48 (2010) 87–91.
[13] W.S. Wan Ngah, L.C. Teong, M.A.K.M. Hanafiah, Adsorption of dyes and heavy metal ions by chitosan composites: a review, Carbohydr. Polym., 83 (2011) 1446–1456.
[14] A.R. Nesic, S.J. Velickovic, D.G. Antonovic, Characterization of chitosan/montmorillonite membranes as adsorbents for Bezactiv Orange V-3R dye, J. Hazard. Mater., 209–210 (2012) 256–263.
[15] L. Bingjie, W. Dongfeng, Y. Guangli, M. Xianghong, Adsorption of heavy metal ions, dyes and proteins by chitosan composites and derivatives - a review, J. Ocean Univ. China, 12 (2013) 500–508.
[16] D.-W. Cho, B.-H. Jeon, C.-M. Chon, F.W. Schwartz, Y. Jeong, H. Song, Magnetic chitosan composite for adsorption of cationic and anionic dyes in aqueous solution, J. Ind. Eng. Chem., 28 (2015) 60–66.
[17] L. Zeng, M. Xie, Q. Zhang, Y. Kang, X. Guo, H. Xiao, Y. Peng, J. Luo, Chitosan/organic rectorite composite for the magnetic uptake of methylene blue and methyl orange, Carbohydr. Polym., 123 (2015) 89–98.
[18] W. Li, Q. Lin, M. Gao, H. Ma, Adsorption studies of Orange II onto polyaniline/bentonite nanocomposites, Water Sci. Technol., 76 (2017) 337–354.
[19] N.N. Bahrudin, M.A. Nawi, S. Sabar, Immobilized chitosan-montmorillonite composite adsorbent and its photocatalytic regeneration for the removal of methyl orange, React. Kinet. Mech. Catal., 126 (2019) 1135–1153.
[20] S.C. Dey, M. Moztahida, M. Sarker, M. Ashaduzzaman, S.M. Shamsuddin, pH-triggered interfacial interaction of kaolinite/chitosan nanocomposites with anionic azo dye, J. Compos. Sci., 3 (2019) 39–50, doi: 10.3390/jcs3020039.
[21] S. Kang, L. Qin, Y. Zhao, W. Wang, T. Zhang, L. Yang, F. Rao, S. Song, Enhanced removal of methyl orange on exfoliated montmorillonite/chitosan gel in presence of methylene blue, Chemosphere, 238 (2020) 124693–124699, doi: 10.1016/j.chemosphere.2019.124693
[22] F.A.R. Pereira, K.S. Sousa, G.R.S. Cavalcanti, D.B. França, L.N.F. Queiroga, I.M.G. Santos, M.G. Fonseca, M. Jaber, Green biosorbents based on chitosan-montmorillonite beads for anionic dye removal, J. Environ. Chem. Eng., 5 (2017) 3309–3318.
[23] S. Kabbadj, M. Hajjaji, A. Alagui, Chitosan-containing organoclays: structural characterization and retention/removal of methylene blue, Desal. Water Treat., 141 (2019) 342–355.
[24] G. Lagaly, Colloid Clay Science, F. Bergaya, B.K.G. Theng, G. Lagaly, Eds., Handbook of Clay Science-Developments in Clay Science, Vol. 1, Elsevier Ltd., Netherlands, 2006, p. 141.
[25] S. Ba, A. Alagui, M. Hajjaji, Retention and release of hexavalent and trivalent chromium by chitosan, olive stone activated carbon, and their blend, Environ. Sci. Pollut. Res., 25 (2018) 19585–19604.
[26] M.N.V.R. Kumar, A review of chitin and chitosan applications, React. Funct. Polym., 46 (2000) 1–27.
[27] J. Brugnerotto, J. Lizardi, F.M. Goycoolea, W. Arguelles-Monal, J. Desbrières, M. Rinaudo, An infrared investigation in relation with chitin and chitosan characterization, Polymer, 42 (2001) 3569–3580.
[28] A. Tolaimate, J. Desbrières, M. Rhazi, A. Alagui, Contribution to the preparation of chitins and chitosans with controlled physico-chemical properties, Polymer, 44 (2003) 7939–7952.
[29] E.N. Bakatula, D. Richard, C.M. Neculita, G.J. Zagury, Determination of point of zero charge of natural organic materials, Environ. Sci. Pollut. Res., 25 (2018) 7823–7833.
[30] R.M.C. Viegas, M. Campinas, H. Costa, M.J. Rosa, How do the HSDM and Boyd's model compare for estimating intraparticle diffusion coefficients in adsorption processes, Adsorption, 20 (2014) 737–746.
[31] X. Zhou, X. Zhou, Calculation of adsorption using the Langmuir equation, Chem. Eng. Commun., 201 (2014) 1459–1467.
[32] K. El Hafid, M. Hajjaji, Geopolymerization of glass- and silicate-containing heated clay, Constr. Build. Mater., 159 (2018) 598–609.
[33] S.L.C. Ferreira, W.N.L. dos Santos, C.M. Quintella, B.B. Neto, J.M. Bosque-Sendra, Doehlert matrix: a chemometric tool for analytical chemistry-review, Talanta, 63 (2004) 1061–1067.
[34] M. Hajjaji, A. Beraa, Y. Coppel, R. Laurent, A.-M Caminade, Adsorption capacity of sodic- and dendrimers-modified stevensite, Clay Miner., 53 (2018) 525–544.
[35] H. Qiu, L. Lv, B.-C. Pan, Q.-J. Zhang, W.-M. Zhang, Q.-X. Zhang, Critical review in adsorption kinetic models, J. Zhejiang Univ. Sci. A, 10 (2009) 716–724.
[36] R. Calvet, Adsorption of organic chemicals in soils, Environ. Health Perspect., 83 (1989) 145–177.
[37] G. Aravinthan, R. Krishnaprasad, Chitin and Its Derivatives for Biomedical Applications, J.G. Ray, J. Kuruvilla, V. George, Eds., Science and Technology for Sustainable development, Allied Publishers Pvt., Ltd., New Delhi, 2006, pp. 317–324.
[38] F. Ahmed, R. Dewani, M.K. Pervez, S.J. Mahboob, S.A. Soomro, Non-destructive FT-IR analysis of mono azo dyes, Bulg. Chem. Commun., 48 (2016) 71–77.
[39] B. Sarkar, Y. Xi, M. Megharaj, R. Naidu, Orange II adsorption on palygorskites modified with alkyl trimethylammonium and dialkyl dimethylammonium bromide-An isothermal and kinetic study, Appl. Clay Sci., 51 (2011) 370–374.
[40] M. Kaur, M. Datta, Adsorption characteristics of acid Orange 10 from aqueous solutions onto montmorillonite clay, Adsorpt. Sci.Technol., 29 (2011) 301–318.
[41] O.A.A. dos Santos, C.Z. Castelli, M.F. Oliveira, A.F. de Almeida Neto, M.G.C. da Silva, Adsorption of synthetic Orange dye wastewater in organoclay, Chem. Eng. Trans., 32 (2013) 307–312.
[42] X. Jin, B. Yu, Z. Chen, Adsorption of Orange II dye in aqueous solution onto surfactant-coated zeolite : characterization, kinetic and thermodynamic studies, J. Colloid Interface Sci., 435 (2014) 15–20.
[43] L. Zhang, L. Chen, X. Liu, W. Zhang, Effective removal of azo-dye Orange II from aqueous solution by zirconium-based chitosan microcomposite adsorbent, RSC Adv., 5 (2015) 93840–93849.
[44] S. Bouzid, A. Khenifi, K. Bennabou, R. Trujillano, M.A. Vicente, Z. Derriche, Removal of orange II by phosphonium-modified Algerian bentonites, Chem. Eng. Commun., 202 (2015) 520–533.
[45] X.-J. Wu, J.-D. Wang, L.-Q. Cao, Characterization and adsorption performance of chitosan/diatomite membranes for Orange G removal, e-Polymers, 16 (2016) 99–109.
[46] Z.A. Sutirman, M.M. Sanagi, K.J. Abd Karim, A. Abu Naim, W.A.W. Ibrahim, Enhanced removal of Orange G from aqueous solutions by modified chitosan beads: performance and mechanism, Int. J. Biol. Macromol., 133 (2019) 1260–1267.